remote sensing

MDPI

Article

Evaluation of Hybrid Models for Maize Chlorophyll Retrieval Using Medium- and High-Spatial-Resolution Satellite Images

Anting Guo [1,2,3], Huichun Ye [1,2,3], Guoqing Li [4], Bing Zhang [1,2,5], Wenjiang Huang [1,2,3,5,*], Quanjun Jiao [1,2], Binxiang Qian [1,2,5] and Peilei Luo [1,2]

1 Key Laboratory of Digital Earth Science, Aerospace Information Research Institute, Chinese Academy of Sciences, Beijing 100094, China
2 International Research Center of Big Data for Sustainable Development Goals, Beijing 100094, China
3 Key Laboratory of Earth Observation of Hainan, Aerospace Information Research Institute, Chinese Academy of Sciences, Sanya 572029, China
4 National Earth Observation Data Center, Aerospace Information Research Institute, Chinese Academy of Sciences, Beijing 100094, China
5 University of Chinese Academy of Sciences, Beijing 100049, China
* Correspondence: huangwj@aircas.ac.cn

Abstract: Accurate estimation of the leaf or canopy chlorophyll content is crucial for monitoring crop growth conditions. Remote sensing monitoring of crop chlorophyll is a non-destructive, large-area, and real-time method that requires reliable retrieval models and satellite data. High-resolution satellite imagery generally has better object recognition capabilities. However, the influence of the spectral and spatial resolution of medium- and high-spatial-resolution satellite imagery on chlorophyll retrieval is currently unexplored, especially in conjunction with radiative transfer models (RTMs). This has important implications for the accurate quantification of crop chlorophyll over large areas. Therefore, the objectives of this study were to establish an RTM for the retrieval of maize chlorophyll and to compare the chlorophyll retrieval capability of the model using medium- and high-spatial-resolution satellite images. We constructed a hybrid model consisting of the PROSAIL model and the Gaussian process regression (GPR) algorithm to retrieve maize leaf and canopy chlorophyll contents (LCC and CCC). In addition, an active learning (AL) strategy was incorporated into the hybrid model to enhance the model's accuracy and efficiency. Sentinel-2 imagery with a spatial resolution of 10 m and 3 m-resolution Planet imagery were utilized for the LCC and CCC retrieval, respectively, using the hybrid model. The accuracy of the model was verified using field-measured maize chlorophyll data obtained in Dajianchang Town, Wuqing District, Tianjin City, in 2018. The results showed that the AL strategy increased the accuracy of the chlorophyll retrieval. The hybrid model for LCC retrieval with 10-band Sentinel-2 without AL had an R^2 of 0.567 and an RMSE of 5.598, and the model with AL had an R^2 of 0.743 and an RMSE of 3.964. Incorporating the AL strategy improved the model performance (R^2 = 0.743 and RMSE = 3.964). The Planet imagery provided better results for chlorophyll retrieval than 4-band Sentinel-2 imagery but worse performance than 10-band Sentinel-2 imagery. Additionally, we tested the model using maize chlorophyll data obtained from Youyi Farm in Heilongjiang Province in 2021 to evaluate the model's robustness and scalability. The test results showed that the hybrid model used with 10-band Sentinel-2 images achieved good accuracy in the Youyi Farm area (LCC: R^2 = 0.792, RMSE = 2.8; CCC: R^2 = 0.726, RMSE = 0.152). The optimal hybrid model was applied to images from distinct periods to map the spatiotemporal distribution of the chlorophyll content. The uncertainties in the chlorophyll content retrieval results from different periods were relatively low, demonstrating that the model had good temporal scalability. Our research results can provide support for the precise management of maize growth.

Keywords: maize; chlorophyll content; hybrid model; PROSAIL; GPR; Sentinel 2; planet

check for updates

Citation: Guo, A.; Ye, H.; Li, G.; Zhang, B.; Huang, W.; Jiao, Q.; Qian, B.; Luo, P. Evaluation of Hybrid Models for Maize Chlorophyll Retrieval Using Medium- and High-Spatial-Resolution Satellite Images. *Remote Sens.* **2023**, *15*, 1784. https://doi.org/10.3390/rs15071784

Academic Editors: Jochem Verrelst and Petya Campbell

Received: 13 February 2023
Revised: 18 March 2023
Accepted: 22 March 2023
Published: 27 March 2023

1. Introduction

Chlorophyll is an essential plant pigment. It converts light energy into chemical energy during photosynthesis [1,2]. At the leaf level, the chlorophyll content largely determines the utilization of incident solar radiation via photosynthesis [3]. At the canopy scale, the chlorophyll content is typically calculated as the product of the leaf area index (LAI) and leaf chlorophyll content (LCC). The canopy chlorophyll content (CCC) can be used to assess the effects of the canopy structure, LAI, and soil background [4,5]. Therefore, the spatiotemporal quantification of the LCC and CCC is essential for monitoring photosynthetic efficiency and health, among others [6,7].

Optical remote sensing can be used to estimate physiological and biochemical parameters, such as chlorophyll, in real time, facilitating crop monitoring and management [8]. Remote-sensing-based chlorophyll estimation methods include empirical statistical models, radiative transfer models (RTMs), and hybrid models [9,10]. (1) Empirical statistical models are linear, polynomial, exponential, or logarithmic models that describe the empirical relationships between the chlorophyll content and sensitive spectral features (spectral bands, vegetation indices, or spectral transformations) [11]. For example, Zhang et al. [12] developed the modified chlorophyll index (MCI) and used empirical statistical methods to estimate the CCC of sugar beets. (2) Chlorophyll retrieval using RTMs has a sound theoretical basis and physical significance. It was used to quantify the relationship between the chlorophyll content and canopy reflectance [13]. The look-up table (LUT)-based physical retrieval method is an RTM retrieval method that relates the simulated spectral reflectance to chlorophyll values using a mathematical algorithm (i.e., cost function) [14]. For example, Chakhvashvili et al. [15] investigated LCC and CCC retrieval using a LUT-based approach with high-spatial-resolution multispectral unmanned aerial vehicle (UAV) data. (3) Hybrid retrieval models typically use RTMs to generate a training dataset, including simulated spectral data and corresponding parameters. A machine learning regression algorithm (MLRA) is used to establish the relationship between the two [16]. This method has high model scalability and computational efficiency and provides accurate estimates of the biophysical parameters [17]. The Gaussian process regression (GPR) method is a commonly used MLRA for hybrid retrieval methods using vegetation parameters [18]. GPR is superior to other MLRAs, such as random forest and neural networks, because it does not require a large training sample size and provides uncertainty estimates of parameter retrieval [19]. In addition, an active learning (AL) strategy was combined with hybrid retrieval methods for vegetation parameter retrieval to improve model performance. AL optimizes the training dataset via intelligent sampling during iterations, improving the model's accuracy and simplicity [20]. For example, Candiani et al. [21] obtained better results for the retrieval of crop LCCs and CCCs using a hybrid model that included AL.

The retrieval performance depends on the ability of satellite sensors to observe surface target features in addition to the model [22]. Data from optical earth observation sensors were used for the spatiotemporal retrieval of vegetation parameters. However, different optical satellite sensors acquire images with different spectral and spatial resolutions, which may lead to different retrieval results of vegetation parameters. Multispectral satellite images are commonly used for inverting vegetation parameters. They include high-spatial-resolution (e.g., WorldView and Planet), medium-spatial-resolution (e.g., Sentinel and Landsat), and coarse-spatial-resolution (e.g., MODIS) images [23]. Medium- and high-spatial-resolution images are more frequently used for the retrieval of vegetation parameters at smaller regional scales. In general, high-spatial-resolution images are less affected by spatial heterogeneity. However, these images are acquired by commercial satellites and are expensive, and the data processing efficiency is low [24]. Planet satellite imagery has a high spatial resolution (3 m) and contains four spectral bands (blue, green, red, and near-infrared (NIR)) [25]. Some researchers used Planet imagery for the retrieval of vegetation parameters. For example, Migolet and Goïta [26] estimated the total aboveground dry biomass of oil palm in the Congo Basin using Planet imagery. Some medium-spatial-resolution satellite images are open-source data and have good spectral and spatial resolutions. Sentinel-2 provides medium-spatial-resolution imagery, enabling the continuous monitoring of vegetation parameters. It has global land surface coverage and a high temporal resolution with a revisit time of 5 d. The images have a ground-sampling distance (GSD) of 10 m and consist of 13 bands, including visible (VIS), red-edge, NIR, and short-wave infrared (SWIR) bands [27]. Numerous researchers used Sentinel 2 imagery for the retrieval of vegetation parameters, including LAI [28], chlorophyll [29], nitrogen [30], and biomass [31]. A multitude of studies employed medium- and high-spatial-resolution satellite imagery for the retrieval of vegetation parameters; however, there remains a lack of research comparing the efficacy of these two types of imagery when integrated with hybrid models in chlorophyll retrieval.

To perform crop chlorophyll retrieval at a regional scale, it is particularly important to construct models with high accuracy and scalability and to explore their capability to incorporate different satellite images. Therefore, we constructed a hybrid model consisting of an RTM and MLRA and performed the retrieval of the LCC and CCC of maize in different growth stages using Sentinel-2 and Planet satellite imagery, respectively. The objectives were (1) to investigate the performance of the hybrid model with the AI strategy for maize chlorophyll retrieval, (2) to evaluate the spatial and temporal scalability of the hybrid model, and (3) to compare the performance of the hybrid model for chlorophyll retrieval using high- and medium-spatial-resolution satellite images (i.e., Planet and Sentinel-2).

2. Materials and Methods

2.1. Study Areas

The study area consisted of two regions. The first was Dajianchang Town in the Wuqing District, Tianjin, China (39°54.20′N, 117°26.90′E) (Figure 1a). Daqinchang town has a warm temperate semi-humid continental monsoon climate, with an annual average temperature of 11.6 °C, cumulative precipitation of 606.8 mm, and sunshine time of 2705 h. The area's topography is relatively flat, and the soil is loose and fertile, making it ideal for crop cultivation and production. The major summer crops in this study area are maize and soybeans, accounting for 78.3% and 8.9% of the total crop area, respectively. Maize is planted successively in fields, facilitating the collection of fields and satellite data. The other study area was located at Youyi Farm, Shuangyashan City, Heilongjiang Province, China (131°28′~132°15′E, 46°31′~46°59′N) (Figure 1a). It is part of the Three Rivers Plain. This area has a mid-temperate continental monsoon climate, with an average annual temperature of 3.1 °C, cumulative temperature of 2170–2700 °C, average sunshine time of 2557 h, average precipitation of 514 mm, and a frost-free period of 143 d. The dominant soil types at Youyi Farm are meadow soil, black soil, and swampy soil, with high soil fertility. Youyi Farm grows crops year-round, primarily soybean, maize, and rice.

2.2. Field Data Acquisition

We established 40 sampling units (SUs) (10 × 10 m) with growth uniformity in the study area in Dajianchang town (Figure 1b) and measured the LCC and LAI of maize in each SU during 31 July–2 August, 15–17 August, and 5–6 September 2018. The data in two SUs could not be measured due to irrigation on 15–17 August. We established 39 SUs (10 × 10 m) with growth uniformity at Youyi Farm and measured the LCC and LAI on 28–29 July 2021. Ultimately, we obtained 30 SUs after eliminating those covered by clouds in the imagery. The LCC was measured using a SPAD-502 chlorophyll meter (Konica Minolta, Tokyo, Japan) [32]. Three maize plants were randomly selected in each SU for the SPAD measurements. All leaves of the maize plants were measured sequentially from top to bottom, and the average of the SPAD values of all leaves of the three maize plants was used as the SPAD value of that SU. The SPAD value is a unitless value that is highly correlated with the LCC, and we converted it to an LCC (μg/cm^2) value using Equation (1), as described by Chakhvashvili et al. [15]. The CCC was calculated from the LCC of each SU multiplied by the LAI (Equation (2)) [21]. The LAI was obtained by harvesting maize leaves through destructive sampling [33]. In addition, the location of each SU was recorded using a differential global positioning system (DGPS). The statistical results of the LCCs and CCCs for all SUs are listed in Table 1.

$$LCC = 9.1411e^{0.0318*SPAD}, \quad (1)$$

$$CCC = LCC * LAI/100, \quad (2)$$

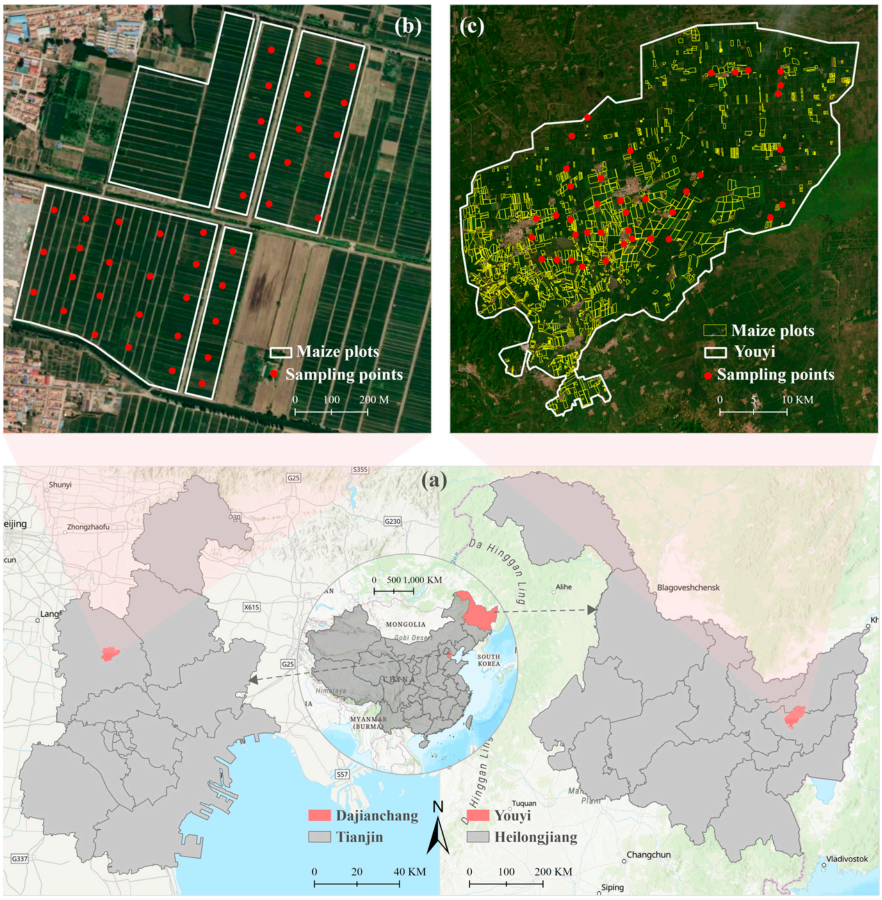

Figure 1. Location of the study area and spatial distribution of sample points: (**a**) locations of the study areas in Dajianchang Town and Youyi Farm; (**b**,**c**) distribution of the sample points in Dajianchang Town and Youyi Farm, respectively (the backgrounds of the maps in (**b**,**c**) are from Google Maps).

Table 1. Statistics of the maize LCCs and CCCs obtained from Dajianchang Town and Youyi Farm.

Study Areas	Parameters	Unit	Number of Samples	Minimum	Maximum	Mean	Standard Deviation
Dajianchang Town	LCC	μg/cm^2	118	18.3	49.66	35.5	7.85
	CCC	g/m^2	118	0.29	2.18	1.20	0.44
Youyi Farm	LCC	μg/cm^2	30	26.52	53.3	36.02	6.22
	CCC	g/m^2	30	0.81	1.92	1.18	0.28

2.3. Satellite Image Acquisition and Processing

Sentinel 2 and Planet images were acquired for the maize chlorophyll retrieval. Sentinel 2 is part of the European Space Agency's Copernicus program. The satellite carries a multispectral imager (MSI) [24]. Sentinel-2 has 13 spectral bands covering the VIS, NIR, and SWIR regions (Table 2). The three 60 m spatial resolution bands designed for the monitored atmospheric conditions (i.e., B1, B9, and B10) were not considered in this study. We obtained

MSI Level 1C images from the ESA website (https://scihub.copernicus.eu/dhus/#/home, accessed on 1 October 2018 and 12 November 2021) for three periods covering Dajianchang town (Table 3) and for six periods covering Youyi Farm. We used the Sen2Cor algorithm in the Sentinel SNAP toolbox to apply atmospheric, radiometric, and topographic corrections to the selected images (Level 1C) to obtain Level 2A images with surface reflectance values [34]. Then, we resampled the images from 20 m resolution to 10 m resolution using bilinear interpolation [35]. In addition, we manually removed the cloud-covered areas from the images of Youyi Farm in the six periods. PlanetScope is a constellation of more than 130 CubeSats that cover the Earth's land surface daily. Planet images contain four spectral bands (blue, green, red, and NIR) with a spatial resolution of 3 m [26]. They were downloaded from the official website (https://www.planet.com/, accessed on 12 November 2021) and atmospherically and radiometrically corrected to obtain surface reflectance products. The selected images were cloud-free, closest to the sample acquisition date, and covered the study area in Dajianchang town (Table 3). In addition, we extracted the spectral information of the Sentinel-2 and Planet images corresponding to the SUs in the ENVI 5.3 software. The spectral information for the Sentinel-2 images was extracted based on the image elements corresponding to the geographic coordinates of the center of each SU. For the Planet images with a spatial resolution of 3 m, we extracted the spectral information of 3 × 3 pixels around the image element corresponding to the geographic coordinates of the SU center and averaged the spectral value of the 3 × 3 pixels as the spectral value of the Planet image corresponding to the SU.

Table 2. Sentinel-2 and Planet band configurations.

Bands	Sentinel-2			Planet		
	Band Center (nm)	**Bandwidth (nm)**	**Spatial Resolution (m)**	**Band Center (nm)**	**Bandwidth (nm)**	**Spatial Resolution (m)**
B1—Coastal aerosol	442	21	60			
B2—Blue	492	66	10	480	60	3
B3—Green	559	36	10	540	90	3
B4—Red	665	31	10	610	80	3
B5—Vegetation red edge	704	16	20			
B6—Vegetation red edge	739	15	20			
B7—Vegetation red edge	780	20	20			
B8—NIR	833	106	10	780	80	3
B8A—Narrow NIR	864	22	20			
B9—Water vapor	943	21	60			
B10—SWIR-cirrus	1377	30	60			
B11—SWIR	1610	94	20			
B12—SWIR	2186	185	20			

Table 3. Sentinel-2 and Planet images acquired of the two study areas.

Study Areas	Satellite Datasets	Acquisition Date					
Dajianchang	Sentinel-2	2018/08/03	2018/08/16	2018/09/05			
	Planet	2018/08/01	2018/08/17	2018/09/04			
Youyi	Sentinel-2	2021/07/03	2021/07/13	2021/07/28	2021/08/17	2021/09/01	2021/09/14

2.4. Hybrid Model for Chlorophyll Retrieval in Maize

The hybrid model for chlorophyll retrieval was established through the integration of the PROSAIL model and GPR. The AL strategy was embedded in the hybrid model to enhance model efficiency. PROSAIL was constructed by coupling the PROSPECT-PRO model at the leaf level [36] and the 4SAIL model at the canopy level [37], and it was used to generate the simulated dataset. The PROSPECT-PRO model describes the optical properties of leaves in the 400–2500 nm range by calculating leaf hemispherical reflectance and transmittance using eight leaf parameters, namely, leaf structure, LCC, leaf carotenoid content, leaf anthocyanin content, leaf water content, leaf protein content, brown pigment content, and carbon-based constituents [10]. The 4SAIL model input variables include LAI, average leaf inclination angle, hot spot parameters, observer zenith angle, solar zenith angle, relative azimuth angle, and soil brightness [38]. The input parameters of the PROSAIL model are listed in Table 4. For the setting of the parameters, the LAI and LCC ranges were set with reference to the measured values, while the rest of the parameters were set with reference to the range of parameters in the literature. The combination of these parameters results in the generation of LUTs with hundreds of thousands of entries. We used the Latin hypercube sampling (LHS) [39] method to select a subset of 1000 entries in the LUT to train the GPR model. Finally, the data were resampled using the spectral bandwidth and the spectral response function of each sensor to match the 10 bands of Sentinel-2 and the 4 bands of Planet.

Table 4. Symbols, units, and parameter ranges of the input parameters of the PROSAIL model.

Model	Parameter	Description	Unit	Distribution	Range
PROSPECT-PRO	N	Leaf structure	Unitless	Uniform	1–2 [17]
	C_{ab}	Leaf chlorophyll content	μg/cm^2	Uniform	10–70
	C_{cx}	Leaf carotenoid content	μg/cm^2	Uniform	2–20 [10]
	C_{anth}	Leaf anthocyanin content	μg/cm^2	Uniform	0–2 [17]
	EWT	Leaf water content	cm	Uniform	0.001–0.02 [17]
	C_p	Leaf protein content	g/cm^2	Uniform	0.001–0.0015 [10]
	C_{brown}	Brown pigment content	μg/cm^2	-	0 [17]
	CBC	Carbon-based constituents	g/cm^2	Uniform	0.001–0.01 [17]
4SAIL	ALA	Average leaf inclination angle	deg	Uniform	20–70 [15]
	LAI	Leaf area index	m^2/m^2	Uniform	0–6
	HOT	Hot spot parameter	m/m	Uniform	0.01–0.5 [15]
	SZA	Solar zenith angle	deg	Uniform	20–35 [21]
	OZA	Observer zenith angle	deg	-	0 [21]
	RAA	Relative azimuth angle	deg	-	0 [21]
	BG	Soil brightness	Unitless	-	0.8 [40]

GPR is a powerful nonparametric probabilistic algorithm based on Bayesian theory [41]. It was successfully used for vegetation parameter retrieval [18,20,42]. GPR provides standard deviations and means of the parameter retrieval values, which were used to calculate coefficients of variation as a measure of retrieval uncertainty [43]. In addition, GPR requires a relatively small amount of training data to establish relationships between the spectra and parameters, corresponding to the number of samples generated by the PROSAIL model. A mathematical description of GPR used for the retrieval of vegetation parameters can be found in Estévez et al. [19].

The AL strategy was used during sample training to optimize the model [44]. It randomly selects a small portion of the sample data from the original LUT to train the GPR model and evaluates its performance using validation data. A new sample is added to a randomly generated initial training dataset, and a new GPR model is trained. If the new sample improves the model accuracy, it is retained in the training pool; otherwise, it is removed. The final result is a training dataset containing samples that can increase the model's performance [10,45]. AL uses two sampling strategies: uncertainty and diversity sampling [46]. The Euclidean distance-based diversity (EBD) is a diversity sampling method that was widely used in recent years. It annotates samples in the pool that are distant from the existing samples in the training set using the squared Euclidean distance [20]. The GPR and AL were implemented in ARTMO's toolbox of MLRAs (https://artmotoolbox, accessed on 12 December 2022).

We constructed three models to compare their performances for chlorophyll retrieval using Sentinel-2 and Planet images: (1) a model using 10 bands of Sentinel-2 images, (2) a model using 4 bands of Sentinel-2 images corresponding to the Planet image bands, and (3) a model using Planet images. We also compared the performances of models with and without AL to verify the effectiveness of this method. For example, the hybrid model with the AL strategy using 10 bands of Sentinel-2 images was labeled S2-10B-AL and the hybrid model without AL was labeled S2-10B. We evaluated the model performance for LCC and CCC retrieval using the coefficient of determination (R^2) and root-mean-square error (RMSE).

2.5. Chlorophyll Mapping Using Multitemporal Sentinel-2 and Planet Images

The hybrid model with optimal performance was used with multi-period Sentinel-2 and Planet images to map the spatial distribution of LCC and CCC of maize in the study area, respectively. Maps depicting the uncertainty maps (i.e., coefficient of variation (CV)) were generated to determine the feasibility of the chlorophyll retrieval results and assess the portability of the model in space and time [47]. We compared the mean and standard deviation of the CV of the retrieval results for different periods. In addition, we manually outlined the maize field boundaries in Dajianchang Town to remove background pixels, such as roads. We extracted the maize fields from the images of Youyi Farm using the maize field boundaries provided by the farm management staff. Theoretically, only image pixels of the maize fields were retained in both study areas to facilitate the mapping of maize chlorophyll.

3. Results

3.1. Hybrid-Model-Based Retrieval of Maize Chlorophyll from Sentinel-2 and Planet Images

The scatterplots (Figure 2) show the measured and retrieved LCCs in Dajianchang Town using the hybrid model and the 2018 Sentinel-2 and Planet images. Figure 2a–c show the retrieval results of the hybrid models without the AL strategy (S2-10B, S2-4B, and PL models, respectively). Figure 2d,e show the retrieval results with the AL strategy. The accuracies of all three models were substantially improved by adding the AL strategy. For example, the evaluation metrics of the S2-10B model (without AL) were R^2 = 0.567 and RMSE = 5.598, and those of the model with AL (S2-10B-AL) were R^2 = 0.743 and RMSE = 3.964. Similarly, the AL strategy improved the CCC retrieval performance of the hybrid model (Figure 3). Figure 3a–c show the results for the three hybrid models without the AL strategy. For instance, the R^2 and RMSE values of the S2-10B model were 0.508 and 0.347, respectively. The R^2 and RMSE values of the model with the AL strategy (S2-10B-AL) were 0.655 and 0.255, respectively (Figure 3d–f). In addition, the 1:1 line and the fitted line in the scatterplot show that overestimation and underestimation of the LCCs occurred in the hybrid model without the AL strategy. The PL model had the largest underestimation (Figure 2c). However, adding AL improved the model performance. The S2-10B model significantly underestimated the CCC values (Figure 3a), and the PL showed underestimations for almost all points (Figure 3c). However, underestimation did not occur in the model with the AL strategy.

The accuracy of the PL-AL model was higher than that of the S2-4B-AL model. For example, in the LCC retrieval, the R^2 of the PL-AL model was 0.723, and the RMSE was 4.131 (Figure 2f); in contrast, the R^2 of the S2-4B-AL model was 0.707, and the RMSE was 4.245 (Figure 2e). In addition, the R^2 of the PL model was higher than that of the S2-4B model for the LCC and CCC retrievals, but the RMSE was lower than that of the S2-4B model. However, the S2-10B-AL and S2-10B models outperformed the PL-AL and PL models in the LCC and CCC retrievals, respectively. For example, the R^2 of the S2-10B-AL model in the CCC retrieval was 0.655 and the RMSE was 0.255 (Figure 3d), whereas the R^2 of PL-AL was 0.624 and the RMSE was 0.266 (Figure 3f). These results indicate that for images with the same spectral bands, higher-spatial-resolution images had advantages in chlorophyll retrieval. However, higher spectral resolution was more advantageous than higher spatial resolution. In addition, the retrieval accuracies of the CCCs were lower than those of the LCCs for different models. We validated the S2-10B-AL model with optimal performance using the sample data acquired at Youyi Farm in 2021. The model had a high accuracy, with R^2 = 0.792 and RMSE = 2.8 for the LCC and R^2 = 0.726 and RMSE = 0.152 for the CCC (Figure 4).

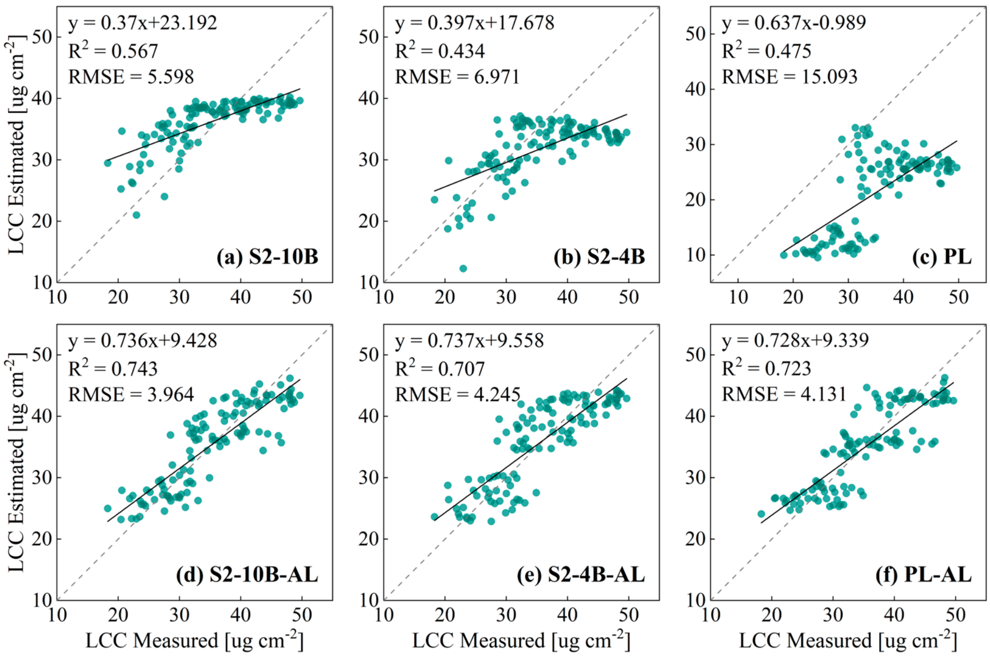

Figure 2. Relationship between the measured and retrieved LCCs in Dajianchang town using the hybrid model and (**a**) Sentinel-2 imagery with 10 bands, (**b**) Sentinel-2 imagery with 4 bands, and (**c**) Planet imagery without the AL strategy; (**d**–**f**) the results using the hybrid model and three types of images with the AL strategy, respectively.

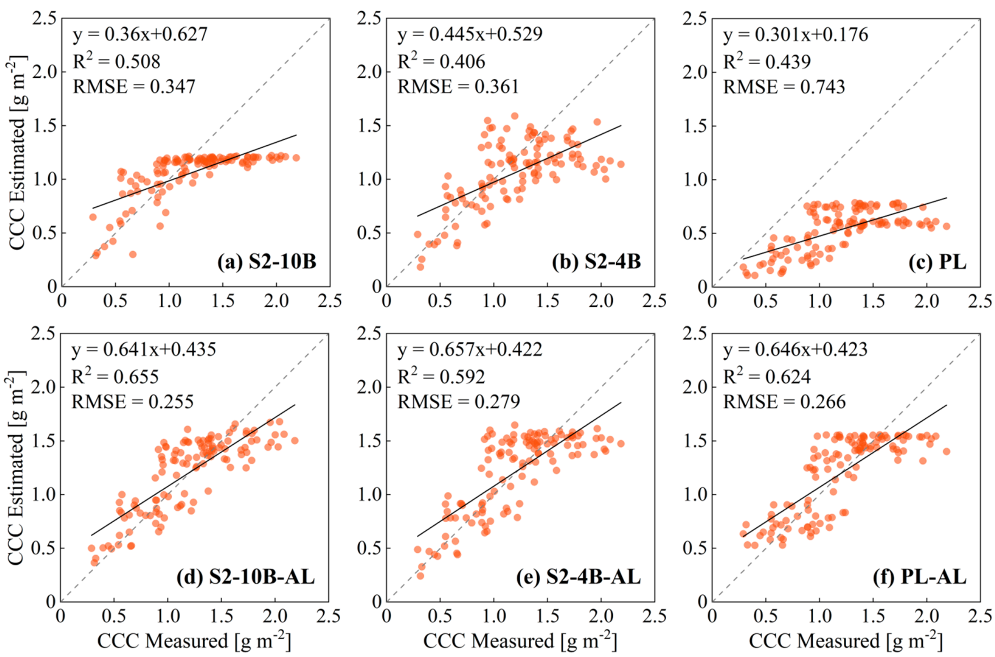

Figure 3. Relationship between the measured and retrieved CCCs in Dajianchang town using the hybrid model and (**a**) Sentinel-2 imagery with 10 bands, (**b**) Sentinel-2 imagery with 4 bands, and (**c**) Planet imagery without the AL strategy; (**d**–**f**) the results using the hybrid model and three types of images with the AL strategy, respectively.

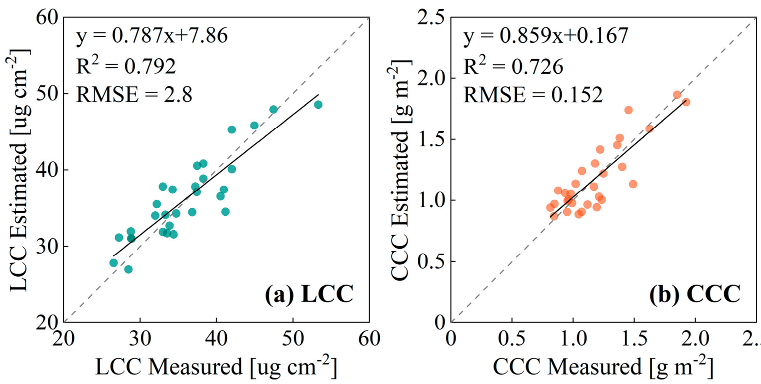

Figure 4. Relationship between the measured and retrieved (**a**) LCCs and (**b**) CCCs at Youyi Farm using the hybrid model with the AL strategy and Sentinel-2 imagery with 10 bands.

3.2. Multi-Period Maize LCC and CCC Spatial Mapping Using Sentinel 2 and Planet Images

The S2-10B-AL and PL-AL models were used to map the spatial and temporal distributions of the LCCs and CCCs during the maize-growing season using multi-period Sentinel-2 and Planet images, respectively (Figures 5 and 6). Figure 5a–c show the spatial distributions of the LCCs in Dajianchang Town on 3 August, 16 August, and 5 September, 2018, using Sentinel-2 images. The mean value of the LCC increased over time (27, 36, and 41 μg/cm^2), which was consistent with the growth pattern of maize. Figure 5d–f show the retrieval results of the LCCs based on the Planet images. The LCC distribution was consistent with the retrieval results based on the Sentinel-2 images. However, the CV values were much lower (lower uncertainty) for the Sentinel-2-image-based retrievals than for the Planet-image-based retrievals (Figure 9a). The mean ± standard deviation of the CV values of the Sentinel-2 image-based LCC retrievals were 6.42 ± 1.65%, 3.47 ± 0.77%, and 4.06 ± 0.78% for the three periods, whereas those of the Planet-image-based retrievals were 45.08 ± 2.03%, 27.58 ± 4.41%, and 22.7 ± 2.88%, respectively. Figure 6a–c show the retrieval maps of the CCCs for the three periods based on the Sentinel-2 images. The mean CCC values for the three periods were 0.758 g/m^2, 1.28 g/m^2, and 1.3 g/m^2, respectively. The CV values were similar for the CCC and LCC retrieval results and were lower for the Sentinel-2 image retrieval results than for the Planet image retrieval results in all three periods. The mean ± standard deviation of the CV values based on the Sentinel-2 image retrieval results in the three periods were 8.17 ± 2.71%, 13.15 ± 2.41%, and 15.57 ± 2.47%, respectively. Those based on the Planet image retrieval results were 46.4 ± 8.2%, 24.54 ± 7.23%, and 20.63 ± 6.75%, respectively. In general, the Sentinel-2 images provided better chlorophyll retrieval results than the Planet images and were more stable in the three periods.

We mapped the maize LCCs and CCCs in six periods using the S2-10B-AL model in the larger study area (Youyi Farm). Figures 7 and 8 show the spatial distributions of the LCCs and CCCs for the six periods, respectively. The chlorophyll content shows an increasing trend over time. However, there was some variability in the chlorophyll content in the study area due to differences in tillage patterns and management levels. Figure 9b shows the uncertainties of the LCC and CCC retrievals for the six periods. The CV values of the retrievals were relatively stable (mean CV values of 10.85–14.88%), except for a large variation in the CV values of the CCC retrievals on September 14 (mean ± standard deviation of the CV of 33.7 ± 14.45%). The CV values of the LCC retrieval were smaller than those of the CCC retrieval, and the range of the mean CV values for the six periods was 5.22–8.68%. These results indicate that the S2-10B-AL model had the best performance and stability in different growth periods of maize.

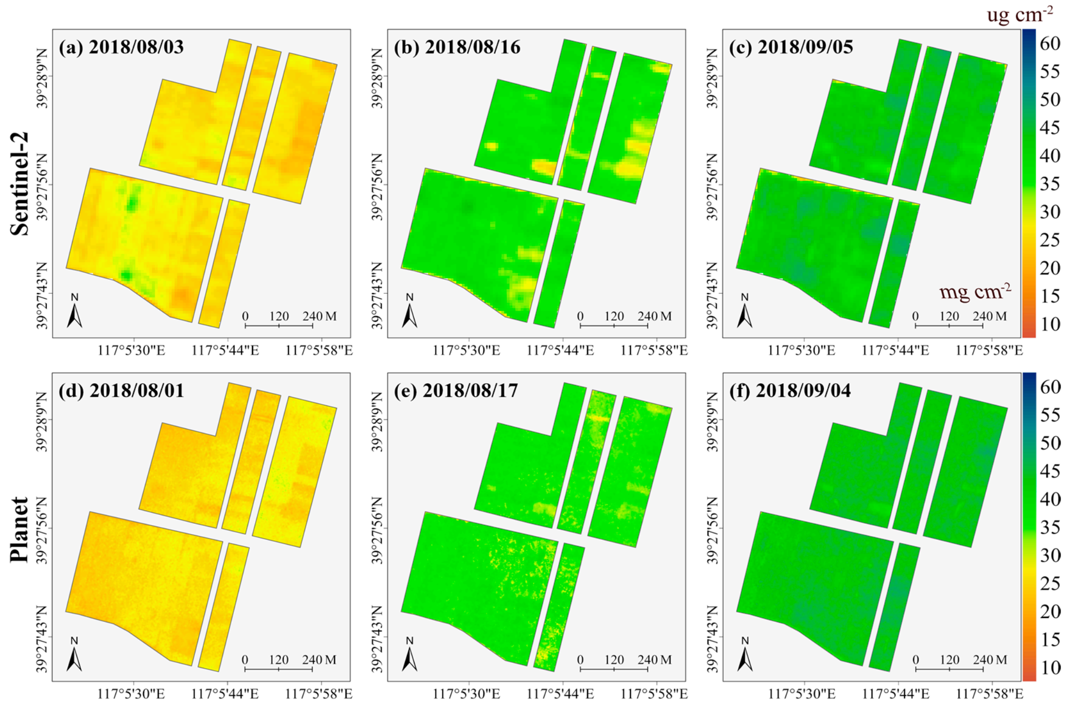

Figure 5. Multi-period maize LCC maps of Dajianchang Town obtained from (**a**–**c**) Sentinel-2 and (**d**–**f**) Planet imagery using the hybrid model.

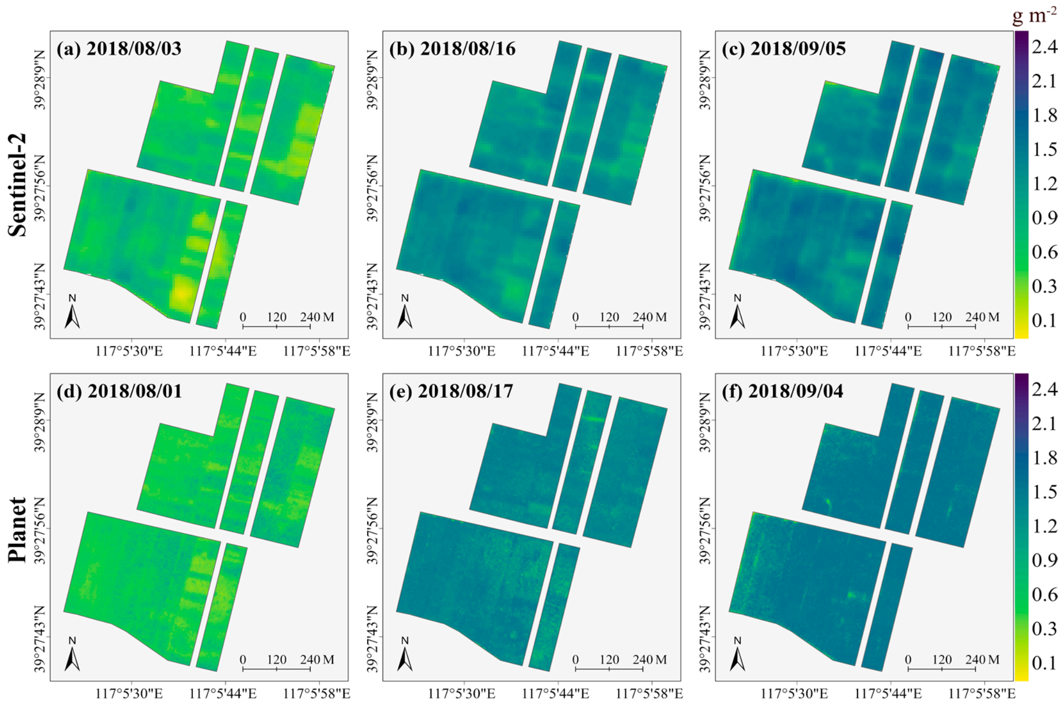

Figure 6. Multi-period maize CCC maps of Dajianchang Town obtained from (**a**–**c**) Sentinel-2 and (**d**–**f**) Planet imagery using the hybrid model.

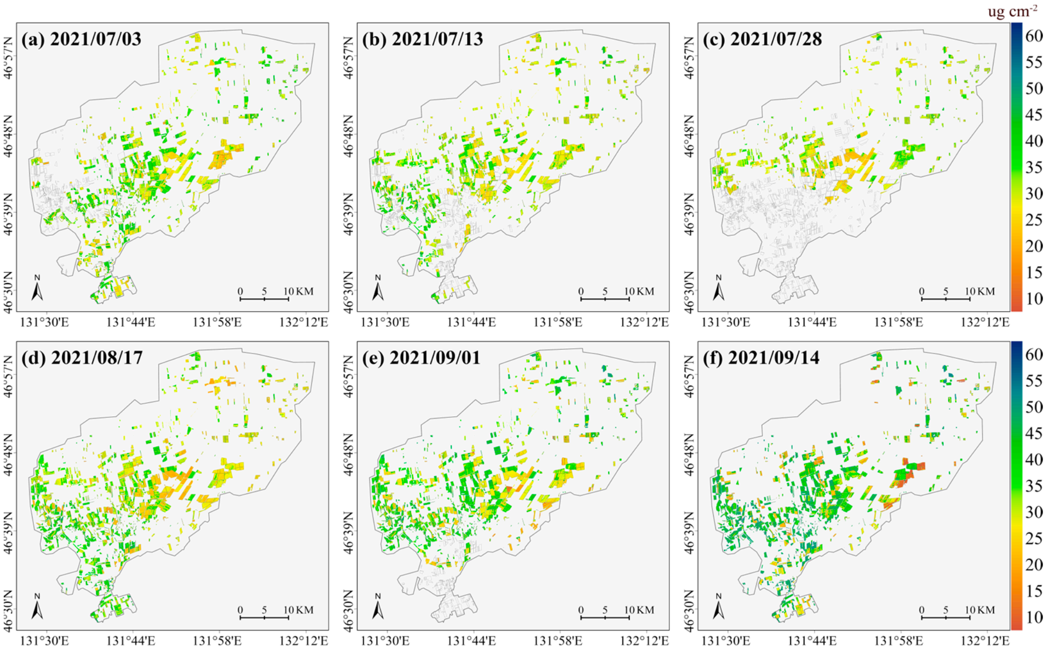

Figure 7. Maize LCC maps of Youyi farm obtained from Sentinel-2 imagery on (**a**) 3 July, (**b**) 13 July, (**c**) 28 July, (**d**) 17 August, (**e**) 1 September and (**f**) 14 September 2021 using the hybrid model.

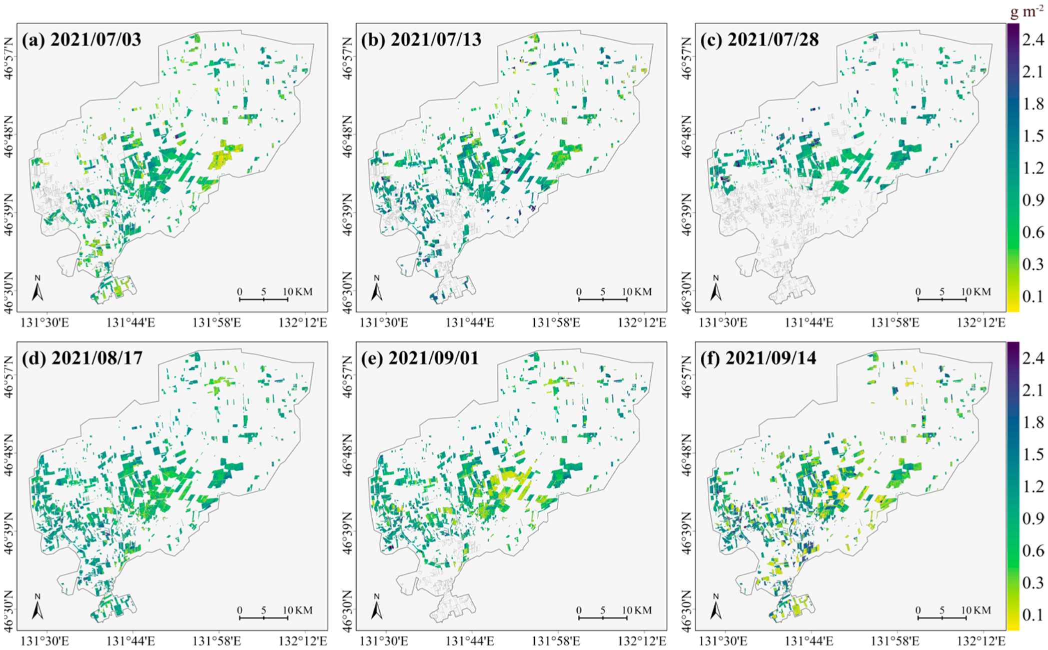

Figure 8. Maize CCC maps of Youyi farm obtained from Sentinel-2 imagery on (**a**) 3 July, (**b**) 13 July, (**c**) 28 July, (**d**) 17 August, (**e**) 1 September and (**f**) 14 September 2021 using the hybrid model.

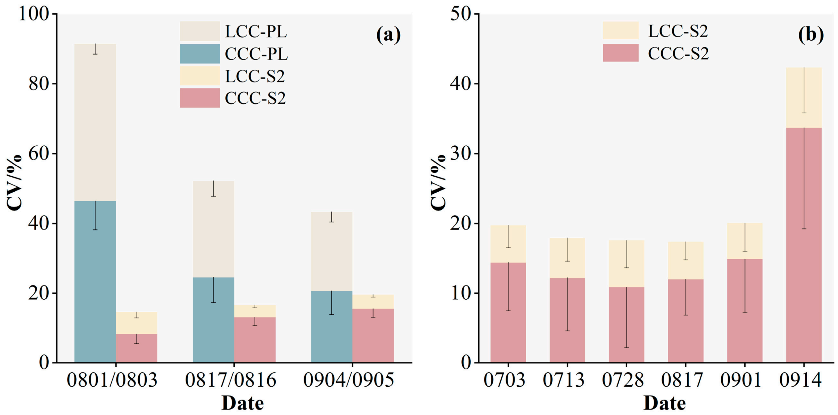

Figure 9. Uncertainties (i.e., CV) associated with chlorophyll retrieval using the hybrid model in different periods in (**a**) Dajianchang Town and (**b**) Youyi Farm.

4. Discussion

We established a hybrid model for maize LCC and CCC retrieval by coupling the PROSAIL model and the GPR algorithm. Good retrieval results were obtained in different growth periods of maize. When crop parameter retrieval is performed in a large or remote area, the number of field samples is often small, limiting the model's accuracy. The training data for the hybrid model was the result of the parameterization of the PROSAIL model, and thus, we only needed a small number of field samples for the tuning of the AL method and the validation of the model. This study confirmed that high-accuracy chlorophyll content estimation could be achieved using only the simulated training dataset generated by the PROSAIL model. Similar results were obtained by Tagliabue et al. [10]. In addition, the number of training data samples generated by the PROSAIL model was only 1000. The choice of a smaller sample dataset was mainly related to the characteristics of GPR, which is more advantageous with a small number of samples. The LUT-based physical retrieval method requires approximately 100,000 simulated samples, substantially reducing the model's efficiency. Berger et al. [45] and Verrelst et al. [48] selected 1000 samples to train the model to perform the retrieval of vegetation parameters and obtained good results.

We incorporated the AL strategy into the hybrid model to improve the model's efficiency and accuracy. The AL strategy performs intelligent sampling and selects a few representative training samples to create efficient and lightweight retrieval models. AL proved to be a successful sampling strategy; our results showed that the accuracy of the LCC and CCC retrieval models with the AL strategy was higher than that of the models using the complete dataset. For example, in the LCC retrieval, the R^2 of the S2-10B model was 0.567 and the RMSE was 5.598. In contrast, the S2-10B-AL model showed better performance (R^2 = 0.743 and RMSE = 3.964). It is worth noting that the model with AL in the CCC retrieval also improved the accuracy of the retrieval in general. However, there was still some saturation in the high-CCC part. The reason for this saturation phenomenon may be that the CCC is derived by multiplying LCC and LAI. This means that a high CCC is related to a complex maize canopy structure, such as a high leaf area index and high leaf area density, and these complex maize canopy structures can complicate the reflectance signal in remotely sensed images, leading to reduced retrieval accuracy [11,49]. In addition, we found that the saturation was significantly lower in the S2-10B-AL model than in the S2-4B-AL and PL-AL models, suggesting that the reduction in spectral information was also an important factor in increasing the saturation. The saturation problem of CCC retrieval has been one of the problems that researchers have been trying to solve, and in the next study, we will also think about how to solve the saturation problem of hybrid models in CCC retrieval. It is important to note that the AL strategy uses field sample data for model training, which may reduce the model's portability. However, we obtained superior results when we applied the hybrid model with the AL strategy to images in different periods and locations for chlorophyll retrieval. For example, the retrievals of the maize LCCs and CCCs for three periods in Dajianchang Town achieved good performances; the uncertainty (i.e., CV) of the LCC retrievals based on Sentinel-2 images was below 10%. Similarly, the CV values ranged from 5.22 to 8.68% in the LCC retrieval results for six periods at Youyi Farm. These results demonstrate the robustness of the hybrid model to temporal and spatial variations. In order to make our hybrid model more convincing, we will then acquire more data from different regions to validate the model. Empirical statistical models using field measurements often have low scalability. The configuration of the proposed hybrid model provides a reference for establishing other scalable models.

We compared the performance of the hybrid model for retrieval using Sentinel-2 and Planet images and found that the LCC and CCC retrievals based on Planet images were superior to those based on the 4-band Sentinel-2 images but lower than those based on the 10-band Sentinel-2 images. In other words, when the Planet and Sentinel-2 images had the same number of bands (i.e., blue, green, red, and NIR bands), the chlorophyll retrieval results were more accurate for images with a higher spatial resolution (i.e., Planet). When the number of bands of the Sentinel-2 images was increased from 4 to 10 (including red-edge bands), the chlorophyll retrieval outperformed that of the Planet images. This finding suggests that high spectral resolution was more critical than high spatial resolution for chlorophyll retrieval when the number of bands was increased. In addition, the uncertainty of the chlorophyll retrieval was much lower for the S2-10B-AL model than for the PL-AL model. The reason for the advantage of the 10-band Sentinel-2 images over the Planet images for chlorophyll retrieval may be two-fold. First, Sentinel 2 images contain three additional red-edge bands that characterize vegetation vigor. The red-edge wavelength reflectance (680–750 nm) increases sharply from the red-band absorption maximum to the NIR shoulder. It is highly sensitive to chlorophyll and exhibits less saturation at a high chlorophyll content [50]. Thus, the chlorophyll retrieval capacity is higher for Sentinel-2 images containing red-edge bands. Second, we excluded the background pixels in the images. Thus, the 10 m-resolution Sentinel-2 images and the 3 m-resolution Planet images contained only maize pixels. Under the conditions of relatively simple and homogeneous maize pixels, the Sentinel-2 images with more rich spectral information had an advantage over Planet images with fewer bands for chlorophyll retrieval. Our results are similar to previous studies. For example, Guo et al. [51] compared UAV, WorldView-2, and Sentinel-2 images to estimate the LAI and found that WorldView-2 images provided the highest estimation accuracy, followed by Sentinel-2 and UAV multispectral images. Although the UAV images had the highest spatial resolution (7 cm), they had only five spectral bands. It is noteworthy that these studies used empirical statistical models to compare the retrieval results of vegetation parameters from different images. In contrast, we conducted the first study that compared the chlorophyll retrieval performance of a hybrid retrieval model using multispectral images with different spatial resolutions. High-spatial-resolution images may provide better feature characterization capabilities in more complex background conditions. In future studies, we will compare satellite images of different resolutions to verify the chlorophyll retrieval capacity of the hybrid model using high-resolution satellite images. For example, in June 2020, Planet Labs released the latest satellite imagery with eight bands [52]. This imagery is richer in spectral information than the four-band imagery used in our study, but its ability to be combined with a hybrid chlorophyll retrieval method is not known. Next, we will try to apply a hybrid model to this image for chlorophyll retrieval. In addition, the method of atmospheric correction during satellite image processing is one of the factors to be considered when comparing the chlorophyll retrieval capabilities of different satellite images. Different atmospheric correction methods may produce different reflectance, which may have an impact on the comparison of chlorophyll retrieval results [53,54]. In the comparison of the two types of satellite imagery in this study, we focused more on the effect of the number of bands and the spatial scale on chlorophyll retrieval. Thus, the atmospheric correction was identified as a default constant. In the next study, we will specifically compare different atmospheric correction methods to assess the effect of atmospheric correction methods on chlorophyll retrieval.

5. Conclusions

We compared for the first time the performance of a hybrid model (PROSAIL and GPR) with an AL strategy for maize chlorophyll retrieval using high-spatial-resolution Planet images and moderate-spatial-resolution Sentinel-2 images. We evaluated the effect of the AL strategy on retrieval performance. The LCC and CCC retrieval accuracies were improved after adding the AL strategy to the hybrid model for Sentinel-2 and Planet images. For example, the R^2 of the S2-10B model was 0.567 and the RMSE was 5.598 for the LCC retrieval, whereas the R^2 of the S2-10B-AL model was 0.743 and the RMSE was 3.964. We compared the chlorophyll retrieval results using 3 m-resolution Planet images and 10 m-resolution Sentinel-2 images. The 4-band Planet images resulted in higher LCC and CCC retrieval accuracies than the 4-band Sentinel-2 image but lower accuracy than the 10-band Sentinel-2 images. These findings indicate that a high spatial resolution of satellite images had an advantage when the number of bands was the same, but a high spectral resolution was more advantageous than a high spatial resolution when the number of bands increased. We mapped the LCCs and CCCs using the S2-10B-AL model in different maize growth stages of maize and found that the uncertainty of the chlorophyll retrieval results was relatively low in different periods, especially for the LCC retrieval. These results demonstrate the good scalability of the model. In summary, incorporating the AL strategy into the hybrid model substantially improved the accuracy of the LCC and CCC retrieval. Using Sentinel-2 images with a high spectral resolution was more advantageous than using Planet images with a high spatial resolution.

Author Contributions: Conceptualization, W.H. and A.G.; methodology, A.G.; software, B.Q.; validation, A.G., P.L. and H.Y.; formal analysis, A.G.; investigation, Q.J.; resources, Q.J.; data curation, A.G.; writing—original draft preparation, A.G.; writing—review and editing, A.G., W.H. and G.L.; supervision, W.H. and B.Z.; project administration, A.G.; funding acquisition, A.G. and W.H. All authors have read and agreed to the published version of the manuscript.

Funding: This research was funded by the National Key R&D Program of China (2021YFB3900501), National Natural Science Foundation of China (42201365, 42071330), Strategic Priority Research Program of the Chinese Academy of Sciences (grant no. XDA28100500), Hainan Provincial Natural Science Foundation of China (422QN349), Hainan Province Science and Technology Special Fund (no. ZDYF2021GXJS038), and Hainan Provincial High-Level Talent Program of Basic and Applied Basic Research Plan in 2019 of China (2019RC363).

Data Availability Statement: Not applicable.

Acknowledgments: The authors gratefully acknowledge ESA for providing the Sentinel-2 data. We thank our colleagues who participated in the field surveys and data collection.

Conflicts of Interest: The authors declare no conflict of interest.

References

1. Qiao, L.; Tang, W.; Gao, D.; Zhao, R.; An, L.; Li, M.; Sun, H.; Song, D. UAV-based chlorophyll content estimation by evaluating vegetation index responses under different crop coverages. *Comput. Electron. Agric.* **2022**, *196*, 106775. [CrossRef]
2. Jay, S.; Maupas, F.; Bendoula, R.; Gorretta, N. Retrieving LAI, chlorophyll and nitrogen contents in sugar beet crops from multi-angular optical remote sensing: Comparison of vegetation indices and PROSAIL inversion for field phenotyping. *Field Crops Res.* **2017**, *210*, 33–46. [CrossRef]
3. Saberioon, M.; Amin, M.; Anuar, A.; Gholizadeh, A.; Wayayok, A.; Khairunniza-Bejo, S. Assessment of rice leaf chlorophyll content using visible bands at different growth stages at both the leaf and canopy scale. *Int. J. Appl. Earth Obs. Geoinf.* **2014**, *32*, 35–45. [CrossRef]
4. De Grave, C.; Pipia, L.; Siegmann, B.; Morcillo-Pallarés, P.; Rivera-Caicedo, J.P.; Moreno, J.; Verrelst, J. Retrieving and validating leaf and canopy chlorophyll content at moderate resolution: A multiscale analysis with the sentinel-3 OLCI sensor. *Remote Sens.* **2021**, *13*, 1419. [CrossRef]

5. Gupta, S.K.; Pandey, A.C. PROSAIL and empirical model to evaluate spatio-temporal heterogeneity of canopy chlorophyll content in subtropical forest. *Model. Earth Syst. Environ.* **2022**, *8*, 2151–2165. [CrossRef]
6. Zhen, J.; Jiang, X.; Xu, Y.; Miao, J.; Zhao, D.; Wang, J.; Wang, J.; Wu, G. Mapping leaf chlorophyll content of mangrove forests with Sentinel-2 images of four periods. *Int. J. Appl. Earth Obs. Geoinf.* **2021**, *102*, 102387. [CrossRef]
7. Sun, J.; Yang, L.; Yang, X.; Wei, J.; Li, L.; Guo, E.; Kong, Y. Using spectral reflectance to estimate the leaf chlorophyll content of maize inoculated with arbuscular mycorrhizal fungi under water stress. *Front. Plant Sci.* **2021**, *12*, 646173. [CrossRef]
8. Verma, B.; Prasad, R.; Srivastava, P.K.; Yadav, S.A.; Singh, P.; Singh, R. Investigation of optimal vegetation indices for retrieval of leaf chlorophyll and leaf area index using enhanced learning algorithms. *Comput. Electron. Agric.* **2022**, *192*, 106581. [CrossRef]
9. Xu, X.; Lu, J.; Zhang, N.; Yang, T.; He, J.; Yao, X.; Cheng, T.; Zhu, Y.; Cao, W.; Tian, Y. Inversion of rice canopy chlorophyll content and leaf area index based on coupling of radiative transfer and Bayesian network models. *ISPRS J. Photogramm. Remote Sens.* **2019**, *150*, 185–196. [CrossRef]
10. Tagliabue, G.; Boschetti, M.; Bramati, G.; Candiani, G.; Colombo, R.; Nutini, F.; Pompilio, L.; Rivera-Caicedo, J.P.; Rossi, M.; Rossini, M. Hybrid retrieval of crop traits from multi-temporal PRISMA hyperspectral imagery. *ISPRS J. Photogramm. Remote Sens.* **2022**, *187*, 362–377. [CrossRef]
11. Sun, Q.; Jiao, Q.; Qian, X.; Liu, L.; Liu, X.; Dai, H. Improving the retrieval of crop canopy chlorophyll content using vegetation index combinations. *Remote Sens.* **2021**, *13*, 470. [CrossRef]
12. Zhang, J.; Tian, H.; Wang, D.; Li, H.; Mouazen, A.M. A novel spectral index for estimation of relative chlorophyll content of sugar beet. *Comput. Electron. Agric.* **2021**, *184*, 106088. [CrossRef]
13. Lu, B.; He, Y. Evaluating empirical regression, machine learning, and radiative transfer modelling for estimating vegetation chlorophyll content using bi-seasonal hyperspectral images. *Remote Sens.* **2019**, *11*, 1979. [CrossRef]
14. Qian, X.; Liu, L. Retrieving crop leaf chlorophyll content using an improved look-up-table approach by combining multiple canopy structures and soil backgrounds. *Remote Sens.* **2020**, *12*, 2139. [CrossRef]
15. Chakhvashvili, E.; Siegmann, B.; Muller, O.; Verrelst, J.; Bendig, J.; Kraska, T.; Rascher, U. Retrieval of Crop Variables from Proximal Multispectral UAV Image Data Using PROSAIL in Maize Canopy. *Remote Sens.* **2022**, *14*, 1247. [CrossRef]
16. Liang, L.; Di, L.; Zhang, L.; Deng, M.; Qin, Z.; Zhao, S.; Lin, H. Estimation of crop LAI using hyperspectral vegetation indices and a hybrid inversion method. *Remote Sens. Environ.* **2015**, *165*, 123–134. [CrossRef]
17. Berger, K.; Verrelst, J.; Féret, J.-B.; Hank, T.; Wocher, M.; Mauser, W.; Camps-Valls, G. Retrieval of aboveground crop nitrogen content with a hybrid machine learning method. *Int. J. Appl. Earth Obs. Geoinf.* **2020**, *92*, 102174. [CrossRef]
18. Estévez, J.; Berger, K.; Vicent, J.; Rivera-Caicedo, J.P.; Wocher, M.; Verrelst, J. Top-of-atmosphere retrieval of multiple crop traits using variational heteroscedastic Gaussian processes within a hybrid workflow. *Remote Sens.* **2021**, *13*, 1589. [CrossRef]
19. Estévez, J.; Salinero-Delgado, M.; Berger, K.; Pipia, L.; Rivera-Caicedo, J.P.; Wocher, M.; Reyes-Muñoz, P.; Tagliabue, G.; Boschetti, M.; Verrelst, J. Gaussian processes retrieval of crop traits in Google Earth Engine based on Sentinel-2 top-of-atmosphere data. *Remote Sens. Environ.* **2022**, *273*, 112958. [CrossRef]
20. Verrelst, J.; Rivera-Caicedo, J.P.; Reyes-Muñoz, P.; Morata, M.; Amin, E.; Tagliabue, G.; Panigada, C.; Hank, T.; Berger, K. Mapping landscape canopy nitrogen content from space using PRISMA data. *ISPRS J. Photogramm. Remote Sens.* **2021**, *178*, 382–395. [CrossRef]
21. Candiani, G.; Tagliabue, G.; Panigada, C.; Verrelst, J.; Picchi, V.; Rivera Caicedo, J.P.; Boschetti, M. Evaluation of Hybrid Models to Estimate Chlorophyll and Nitrogen Content of Maize Crops in the Framework of the Future CHIME Mission. *Remote Sens.* **2022**, *14*, 1792. [CrossRef] [PubMed]
22. Fernández-Guisuraga, J.M.; Verrelst, J.; Calvo, L.; Suárez-Seoane, S. Hybrid inversion of radiative transfer models based on high spatial resolution satellite reflectance data improves fractional vegetation cover retrieval in heterogeneous ecological systems after fire. *Remote Sens. Environ.* **2021**, *255*, 112304. [CrossRef] [PubMed]
23. Marshall, M.; Thenkabail, P. Advantage of hyperspectral EO-1 Hyperion over multispectral IKONOS, GeoEye-1, WorldView-2, Landsat ETM+, and MODIS vegetation indices in crop biomass estimation. *ISPRS J. Photogramm. Remote Sens.* **2015**, *108*, 205–218. [CrossRef]
24. Heenkenda, M.K.; Joyce, K.E.; Maier, S.W.; de Bruin, S. Quantifying mangrove chlorophyll from high spatial resolution imagery. *ISPRS J. Photogramm. Remote Sens.* **2015**, *108*, 234–244. [CrossRef]
25. Helman, D.; Bahat, I.; Netzer, Y.; Ben-Gal, A.; Alchanatis, V.; Peeters, A.; Cohen, Y. Using Time Series of High-Resolution Planet Satellite Images to Monitor Grapevine Stem Water Potential in Commercial Vineyards. *Remote Sens.* **2018**, *10*, 1615. [CrossRef]
26. Migolet, P.; Goïta, K. Evaluation of FORMOSAT-2 and PlanetScope Imagery for Aboveground Oil Palm Biomass Estimation in a Mature Plantation in the Congo Basin. *Remote Sens.* **2020**, *12*, 2926. [CrossRef]
27. Soriano-González, J.; Angelats, E.; Martínez-Eixarch, M.; Alcaraz, C. Monitoring rice crop and yield estimation with Sentinel-2 data. *Field Crops Res.* **2022**, *281*, 108507. [CrossRef]
28. Estévez, J.; Vicent, J.; Rivera-Caicedo, J.P.; Morcillo-Pallarés, P.; Vuolo, F.; Sabater, N.; Camps-Valls, G.; Moreno, J.; Verrelst, J. Gaussian processes retrieval of LAI from Sentinel-2 top-of-atmosphere radiance data. *ISPRS J. Photogramm. Remote Sens.* **2020**, *167*, 289–304. [CrossRef]
29. Qian, B.; Ye, H.; Huang, W.; Xie, Q.; Pan, Y.; Xing, N.; Ren, Y.; Guo, A.; Jiao, Q.; Lan, Y. A sentinel-2-based triangular vegetation index for chlorophyll content estimation. *Agric. For. Meteorol.* **2022**, *322*, 109000. [CrossRef]

30. Sharifi, A. Using sentinel-2 data to predict nitrogen uptake in maize crop. *IEEE J. Sel. Top. Appl. Earth Obs. Remote Sens.* **2020**, *13*, 2656–2662. [CrossRef]
31. Puliti, S.; Hauglin, M.; Breidenbach, J.; Montesano, P.; Neigh, C.; Rahlf, J.; Solberg, S.; Klingenberg, T.; Astrup, R. Modelling above-ground biomass stock over Norway using national forest inventory data with ArcticDEM and Sentinel-2 data. *Remote Sens. Environ.* **2020**, *236*, 111501. [CrossRef]
32. Mao, Z.-H.; Deng, L.; Duan, F.-Z.; Li, X.-J.; Qiao, D.-Y. Angle effects of vegetation indices and the influence on prediction of SPAD values in soybean and maize. *Int. J. Appl. Earth Obs. Geoinf.* **2020**, *93*, 102198. [CrossRef]
33. Fang, H.; Baret, F.; Plummer, S.; Schaepman-Strub, G. An overview of global leaf area index (LAI): Methods, products, validation, and applications. *Rev. Geophys.* **2019**, *57*, 739–799. [CrossRef]
34. Adeluyi, O.; Harris, A.; Verrelst, J.; Foster, T.; Clay, G.D. Estimating the phenological dynamics of irrigated rice leaf area index using the combination of PROSAIL and Gaussian Process Regression. *Int. J. Appl. Earth Obs. Geoinf.* **2021**, *102*, 102454. [CrossRef]
35. Aguirre-Gutiérrez, J.; Rifai, S.; Shenkin, A.; Oliveras, I.; Bentley, L.P.; Svátek, M.; Girardin, C.A.J.; Both, S.; Riutta, T.; Berenguer, E.; et al. Pantropical modelling of canopy functional traits using Sentinel-2 remote sensing data. *Remote Sens. Environ.* **2021**, *252*, 112122. [CrossRef]
36. Féret, J.-B.; Berger, K.; De Boissieu, F.; Malenovský, Z. PROSPECT-PRO for estimating content of nitrogen-containing leaf proteins and other carbon-based constituents. *Remote Sens. Environ.* **2021**, *252*, 112173. [CrossRef]
37. Verhoef, W.; Jia, L.; Xiao, Q.; Su, Z. Unified optical-thermal four-stream radiative transfer theory for homogeneous vegetation canopies. *IEEE Trans. Geosci. Remote Sens.* **2007**, *45*, 1808–1822. [CrossRef]
38. Danner, M.; Berger, K.; Wocher, M.; Mauser, W.; Hank, T. Efficient RTM-based training of machine learning regression algorithms to quantify biophysical & biochemical traits of agricultural crops. *ISPRS J. Photogramm. Remote Sens.* **2021**, *173*, 278–296.
39. Haboudane, D.; Miller, J.R.; Pattey, E.; Zarco-Tejada, P.J.; Strachan, I.B. Hyperspectral vegetation indices and novel algorithms for predicting green LAI of crop canopies: Modeling and validation in the context of precision agriculture. *Remote Sens. Environ.* **2004**, *90*, 337–352. [CrossRef]
40. Sun, B.; Wang, C.; Yang, C.; Xu, B.; Zhou, G.; Li, X.; Xie, J.; Xu, S.; Liu, B.; Xie, T. Retrieval of rapeseed leaf area index using the PROSAIL model with canopy coverage derived from UAV images as a correction parameter. *Int. J. Appl. Earth Obs. Geoinf.* **2021**, *102*, 102373. [CrossRef]
41. Williams, C.K.; Rasmussen, C.E. *Gaussian Processes for Machine Learning*; MIT Press: Cambridge, MA, USA, 2006; Volume 2.
42. Sinha, S.K.; Padalia, H.; Dasgupta, A.; Verrelst, J.; Rivera, J.P. Estimation of leaf area index using PROSAIL based LUT inversion, MLRA-GPR and empirical models: Case study of tropical deciduous forest plantation, North India. *Int. J. Appl. Earth Obs. Geoinf.* **2020**, *86*, 102027. [CrossRef] [PubMed]
43. Abdelbaki, A.; Schlerf, M.; Retzlaff, R.; Machwitz, M.; Verrelst, J.; Udelhoven, T. Comparison of Crop Trait Retrieval Strategies Using UAV-Based VNIR Hyperspectral Imaging. *Remote Sens.* **2021**, *13*, 1748. [CrossRef] [PubMed]
44. Settles, B. *Active Learning Literature Survey*; Computer Sciences Technical Report 1648; University of Wisconsin–Madison: Madison, WI, USA, 2009.
45. Berger, K.; Rivera Caicedo, J.P.; Martino, L.; Wocher, M.; Hank, T.; Verrelst, J. A survey of active learning for quantifying vegetation traits from terrestrial earth observation data. *Remote Sens.* **2021**, *13*, 287. [CrossRef] [PubMed]
46. Verrelst, J.; Dethier, S.; Rivera, J.P.; Munoz-Mari, J.; Camps-Valls, G.; Moreno, J. Active learning methods for efficient hybrid biophysical variable retrieval. *IEEE Geosci. Remote Sens. Lett.* **2016**, *13*, 1012–1016. [CrossRef]
47. Camps-Valls, G.; Verrelst, J.; Munoz-Mari, J.; Laparra, V.; Mateo-Jimenez, F.; Gomez-Dans, J. A survey on Gaussian processes for earth-observation data analysis: A comprehensive investigation. *IEEE Geosci. Remote Sens. Mag.* **2016**, *4*, 58–78. [CrossRef]
48. Verrelst, J.; Berger, K.; Rivera-Caicedo, J.P. Intelligent sampling for vegetation nitrogen mapping based on hybrid machine learning algorithms. *IEEE Geosci. Remote Sens. Lett.* **2020**, *18*, 2038–2042. [CrossRef]
49. Gitelson, A.A. Wide dynamic range vegetation index for remote quantification of biophysical characteristics of vegetation. *J. Plant Physiol.* **2004**, *161*, 165–173. [CrossRef]
50. Zhang, H.; Li, J.; Liu, Q.; Lin, S.; Huete, A.; Liu, L.; Croft, H.; Clevers, J.G.; Zeng, Y.; Wang, X. A novel red-edge spectral index for retrieving the leaf chlorophyll content. *Methods Ecol. Evol.* **2022**, *13*, 2771–2787. [CrossRef]
51. Guo, X.; Wang, M.; Jia, M.; Wang, W. Estimating mangrove leaf area index based on red-edge vegetation indices: A comparison among UAV, WorldView-2 and Sentinel-2 imagery. *Int. J. Appl. Earth Obs. Geoinf.* **2021**, *103*, 102493. [CrossRef]
52. Tu, Y.-H.; Johansen, K.; Aragon, B.; El Hajj, M.M.; McCabe, M.F. The radiometric accuracy of the 8-band multi-spectral surface reflectance from the planet SuperDove constellation. *Int. J. Appl. Earth Obs. Geoinf.* **2022**, *114*, 103035. [CrossRef]
53. Frazier, A.E.; Hemingway, B.L. A technical review of planet smallsat data: Practical considerations for processing and using planetscope imagery. *Remote Sens.* **2021**, *13*, 3930. [CrossRef]
54. Al Shehhi, M.R.; Gherboudj, I.; Zhao, J.; Ghedira, H. Improved atmospheric correction and chlorophyll-a remote sensing models for turbid waters in a dusty environment. *ISPRS J. Photogramm. Remote Sens.* **2017**, *133*, 46–60. [CrossRef]